

**Atmospheric Transmission at Microwaves (ATM):
An Improved Model for mm/submm Applications**

J.R. Pardo, J. Cernicharo & E. Serabyn

2001-2

To Appear in

IEEE Transactions on Antennas and Propagation

Atmospheric Transmission at Microwaves (ATM): An Improved Model for mm/submm applications

J. R. Pardo, J. Cernicharo, E. Serabyn

J. R. Pardo and J. Cernicharo are with the Division of Physics, Mathematics and Astronomy of California Institute of Technology, MS 320-47, Pasadena, CA 91125, USA (e-mail: pardo@submm.caltech.edu), and with the Instituto de Estructura de la Materia, Dpto. de Física Molecular, CSIC, Madrid, Spain.

E. Serabyn is with the Division of Physics, Mathematics and Astronomy of the California Institute of Technology, Pasadena, California.

Abstract

We present a model of the longwave atmospheric spectrum which improves in many respects widely used old models such as MPM (Liebe et al.) since it is based on recent broadband measurements and calculations. The model is applicable from 0 to 10 THz, its primary goal being to simulate the mm/submm region accessible from the ground (frequencies up to ~ 2 THz at most, with a few windows between 1 and 2 THz accessible only under exceptional conditions in some sites). So far it has been validated from 170 to 1200 GHz by means of ground-based Fourier Transform Spectroscopy measurements on Mauna Kea (Hawaii). Line-by-line calculations of the resonant part of the absorption are performed using a line data base generated from the latest available spectroscopic constants for all relevant atmospheric species. The collisional line widths are obtained from published laboratory data. The excess of absorption in the longwave range that cannot be explained by the resonant spectrum is modeled by introducing two different continuum-like terms based on our own recent measurements: collision-induced absorption of the dry atmosphere due to the electric quadrupole interaction of symmetric molecules (N_2 and O_2), and continuum-like water vapor opacity. All H_2O lines up to 10 THz are included in order to correctly account for the whole H_2O far-wing opacity below 2 THz. Hence, this contribution does not need to be included in a pseudo-continuum term (in contrast to other models used to date). Phase delays near H_2O and O_2 resonances are also important for ground-based astronomy since they affect interferometric phase. The frequency-dependent phase delay function is formally related to the absorption line shape via the Kramers-Krönig dispersion theory, and this relation has been used for modeling those delays. Precise calculations of phase delays are essential for the future Atacama Large Millimeter Array (ALMA) project.

A software package called ATM (*Atmospheric Transmission at Microwaves*) has been developed to provide the radioastronomy and aeronomy communities with an updated tool to compute the atmospheric spectrum in clear-sky conditions for various scientific applications. In this paper we use this model to provide detailed simulations of atmospheric transmission and phase dispersion for several sites suitable for submillimeter astronomy.

Keywords

Atmospheric measurements, Submillimeter wave spectroscopy, Software packages, Radio astronomy.

I. INTRODUCTION

Accurate modeling of the longwave emission/absorption spectrum of the terrestrial atmosphere is needed in many scientific applications. In the astrophysical domain, it is needed to predict the atmospheric attenuation at a given frequency for ground-based

and airborne observatories, to calculate system noise temperatures and to estimate phase delays for interferometry. In remote sensing of the atmosphere and the Earth's surface, obtaining useful data for meteorological and environmental studies relies upon an accurate knowledge of the atmospheric spectrum.

In the longwave domain several models have been widely used to date. The astrophysical community has mainly used the following models: AT (*Atmospheric Transmission*; Grossman^[1], 1989), ATM (*Atmospheric Transmission at Microwaves*; Cernicharo^{[2],[3]}, 1985, 1988, Pardo^[4], 1996), several codes developed on the basis of H.J. Liebe's^{[5],[6]} MPM (Microwave Propagation Model, 1989, 1993), which is also extensively used by the aeronomy and remote sensing communities, and radiative transfer codes based on different well known line data bases: HITRAN (Rothman et al^[7], 1992), JPL (Pickett et al^[8], 1998) and GEISA (Jacquinet-Husson et al^[9], 1999).

Most of the above models do not provide a high degree of accuracy, or are incomplete, for two principal reasons: lack of correct description of the continuum-like opacity and lack of consideration of phase dispersion. The model we present here is the result of several years of work on both the modeling and the experimental sides, and is aimed at computing opacity, radiance, phase delay and polarization along a given path in the terrestrial atmosphere at millimeter and submillimeter wavelengths. Polarization can be produced by different mechanisms such as emission of paramagnetic molecules such as O₂ under the effect of the geomagnetic field, by radiation scattering by hydrometeors, or by reflection on a Fresnel-like (ocean) surface. These mechanisms are also treated in the ATM model but have been (Pardo et al^{[10],[11],[12]}, 1995, 1998, 2000 [Zeeman effect]) or will be discussed elsewhere (Pardo et al^[13], 2001 [scattering by hydrometeors]). Here we discuss only unpolarized radiative transfer through a clear sky.

In section 2 we give an overview of the unpolarized radiative transfer theory, giving some definitions that will be used throughout this paper. The basic theoretical aspects regarding calculations of the resonant absorption of the atmosphere are given in section 3. Different spectroscopic parameters are reviewed in section 4. A discussion comparing our formulation to the widely used MPM models (H.J. Liebe^{[5],[6]}, 1989, 1993) is given in section 5 to show how our treatment improves those works (Liebe's empirical models are otherwise

difficult to link to the quantum mechanical properties of the molecules considered in the models). Line shapes are discussed in section 6. The non-resonant absorption is treated in section 7. We will present some results of our FTS experiments on Mauna Kea in section 8 as a validation of the model. Section 9 then focuses on the astrophysical utility of the code. In particular, it is used to predict atmospheric attenuation, atmospheric emissivity, and phase delay over a wide range of frequencies for several potential and present submillimeter observatory sites. Finally, section 10 provides a summary.

II. UNPOLARIZED RADIATIVE TRANSFER

The unpolarized radiative transfer in non-scattering media is described by a relatively simple differential scalar equation (see Chandrasekar^[14], 1960):

$$\frac{dI_\nu(\vec{r}, \vec{n})}{ds} = \epsilon_\nu - \kappa_\nu I_\nu(\vec{r}, \vec{n}) \quad (1)$$

where I_ν is the radiance (in $\text{W m}^{-2}\text{ster}^{-1}\text{cm}^{-1}$), $\epsilon_\nu d\omega d\nu ds d\sigma$ and $\kappa_\nu I(\vec{r}, \vec{n}, \nu) d\omega d\nu ds d\sigma$ are the amounts of energy emitted and absorbed at frequency ν in a pencil of solid angle $d\omega$ in the direction \vec{r} through a cylinder of length ds and cross-section $d\vec{\sigma} = d\sigma \vec{n}$. ϵ_ν and κ_ν are the macroscopic absorption and emission coefficients. The absorption coefficient gives the fractional loss of intensity (at a given wavelength) per length through an absorbing medium.

After rearranging equation 1 and considering absence of scattering, the radiative transfer problem is unidimensional in the direction of \vec{r} . We can formulate the problem under *Local Thermal Equilibrium* (LTE) conditions as follows:

$$\frac{dI_\nu(s')}{d\tau_\nu} = -I_\nu(s') + S_\nu(T[s']) \quad (2)$$

where s' is a coordinate along the path, $S_\nu = \epsilon_\nu/\kappa_\nu$ is the so-called *source function*, and $d\tau_\nu = \kappa_\nu ds$ is the *differential opacity*. The solution of this equation can be given in an integral form:

$$I_\nu(s) = I_\nu(0)e^{-\tau_\nu(0,s)} + \int_0^s S_\nu(s')e^{-\tau_\nu(s',s)}\kappa_\nu(s')ds' \quad (3)$$

For ground based measurements $I_\nu(0)$ is commonly taken as the radiance from the *cosmic background* (CBR).

However, to actually solve the last equation, a complete knowledge of κ_ν as a function of position, which implies a knowledge of the abundance properties of all contributing molecules, and of the pressure broadening lineshape, is needed. To perform radiative transfer calculations through the atmosphere in particular situations, some well known physical approximations can be assumed. For example, the physical medium under study contains only $\sim 0.001\%$ of its mass above an altitude of 90 km, where in addition, most molecules are strongly dissociated due to solar UV radiation, thus limiting the vertical range needed for the calculations. Only for O_2 Zeeman splitting calculations do we consider higher altitudes (see Pardo et al.^{[10],[11]}, 1995, 1998). Furthermore, within the 0-90 km vertical range, typical temperatures are ~ 220 to 320 K and typical pressures range from ~ 1020 to 0.0015 mb. Under these physical conditions the populations of the different energy levels of a given species in a small volume of atmospheric gas are fully controlled by collisions, and thus depend only on the local physical temperature T (the Local Thermodynamic Equilibrium, or LTE approximation). Collisional rates fall with altitude and pumping by solar photons will start to dominate the population of the molecular levels at some point above the high mesosphere (>80 km) making the LTE approximation fail. At these altitudes, however, the contribution from the different molecular species to the atmospheric opacity in the millimeter, submillimeter and far-infrared wavelength domains is negligible.

To compute the output radiance arising from a propagation path in the atmosphere we need to know the functions $T(s)$ (physical temperature along the path, which determines the local source function and also enters into the absorption coefficient (see equation 10), $P(s)$, and the number densities of the different atmospheric gases $N_i(s)$. We divide the total path into a number of steps and then discretize the integral for numerical calculations to achieve an accuracy of the order of 0.1 K. The geometry for calculations can be plane-parallel for zenith (or nadir) angles up to $\sim 75^\circ$. A spherical geometry must be considered for higher zenith (or nadir) angles and for limb paths, which our model can also provide. At the end the code converts the output radiance I_ν into an equivalent blackbody temperature

$T_{EBB,\nu}$ simply by inverting the Planck function:

$$T_{EBB,\nu} = \frac{h\nu}{k(\ln \frac{2h\nu^3}{I_\nu c^2} + 1)} \quad (4)$$

III. RESONANT ABSORPTION: GENERALITIES

Unless otherwise indicated the units used in this paper and internally in the code are the following:

- Frequency: GHz.
- Pressure: mb.
- Temperature: K.
- Absorption: m^{-1} .
- Phase delay: $\text{deg}\cdot\text{m}^{-1}$.
- Spectroscopic constants: MHz.
- Electric or magnetic dipole moments: Debyes (1 Debye= 10^{-21} esu·m).

In general, the line-by-line integrated opacity corresponding to a path through the terrestrial atmosphere is calculated as follows:

$$\tau_\nu = \sum_{i(\text{layers})} [\sum_{j(\text{molec.})} (\sum_{k(\text{resonances})} \kappa_{\nu_k})_j]_i \cdot \Delta s_i \quad (5)$$

where Δs_i is the path through the homogeneous i -th layer and no line coupling between different species is assumed. As pressure increases the program uses thinner layers to follow the opacity distribution.

Let us consider the process of resonant absorption between two energy levels l and u . In principle it takes place only at the resonant frequency $\nu_{l \rightarrow u}$ and each photon absorbed or emitted corresponds to a loss or gain of one quantum of energy $h\nu_{l \rightarrow u}$. So:

$$dI_{\nu_{l \rightarrow u}} = -(\frac{N_l}{g_l} - \frac{N_u}{g_u}) R_{l \rightarrow u} h\nu_{l \rightarrow u} ds \quad (6)$$

where $R_{l \rightarrow u}$ is the transition rate for $l \rightarrow u$, $N_{l,u}$ are the populations of the energy levels and $g_{l,u}$ their degeneracies. From the microphysical point of view this rate equals to $B_{l \rightarrow u} I_{\nu_{l \rightarrow u}} / c$ where $B_{l \rightarrow u}$ is the Einstein transition coefficient for stimulated absorption, given by (see for example Kroto^[15], 1975):

$$B_{l \rightarrow u} = \frac{2\pi}{3\hbar^2} |\langle u | \mu | l \rangle|^2 \quad (7)$$

where μ is the dipole operator of the transition and $|u\rangle$, $|l\rangle$ are the wavefunctions of the upper and lower states. Finally we have to take into account that several line broadening processes spread the absorptions around the theoretical resonant frequency $\nu_{l \rightarrow u}$. This is taken into account by introducing a line shape function $f(\nu, \nu_{l \rightarrow u})$. The absorption coefficient of an electric dipole (E1) resonance is thus becomes:

$$(\kappa_\nu)_{lu} = \frac{8\pi^3\nu}{3hc} \left[\frac{N_l}{g_l} - \frac{N_u}{g_u} \right] |\langle u | \mu | l \rangle|^2 f(\nu, \nu_{l \rightarrow u}) \quad (8)$$

The last equation is general and we will now discuss its various parts in order to arrive at the formulation actually used in our code.

The collisional relaxation rate under the considered atmospheric conditions is fast enough to maintain a Boltzmann distribution of the energy level populations (see section II). The Boltzmann equation under equilibrium conditions indicates: $\frac{N_u}{g_u} = \frac{N_l}{g_l} \exp[-(E_u - E_l)/KT]$ and the fractional population of molecules in the n-th state is given by:

$$\frac{N_n}{N} = g_n \frac{\exp(-E_n/KT)}{Q} \quad (9)$$

E_n being the energy level of the state and g_n its degeneracy. Q is the partition function [$Q = \sum_i g_i \exp(-E_i/KT)$]. In the case of the Born-Oppenheimer approximation (which holds for the relatively simple molecules to be considered in the atmosphere) the wavefunction is the product of electronic, vibrational, rotational and nuclear spin functions. So, we can apply to the population of a given molecular species the product of vibrational and rotational partition functions. Introducing equation 9 into 8 we have:

$$(\kappa_\nu)_{lu} = \frac{8\pi^3 N \nu}{3hcQ} (e^{-E_l/KT} - e^{-E_u/KT}) \cdot |\langle u | \mu | l \rangle|^2 f(\nu, \nu_{l \rightarrow u}) \quad (10)$$

where N is the number density in the relevant vibrational state of the molecule in question. This is the basic expression used in our model.

IV. SPECTROSCOPIC PARAMETERS

We discuss in this section the calculation of the different parts of equation 10 that we have performed to create the data base used in the model. Only a few parameters have been taken from other existing data bases (see below).

The intensity of the transitions is determined by the matrix elements of the dipole moment (transition probabilities) and by the population factors. Both transition probabilities as well as rotational energy levels (from which both resonance frequencies and population factors under LTE can be determined) can be obtained from the rotational Hamiltonians. This allows us to build a compact data base since spectroscopic line parameters can be derived from a small number of parameters, the rotational constants of the molecular species.

The number of rotational constants to be considered varies for linear molecules, symmetric top molecules, and general asymmetric rotors (the types of molecules we find in the atmosphere). The expressions for those Hamiltonians that we have considered are:

- **Diatomic or linear molecules (with no magnetic moment)**: The rigid rotor Hamiltonian $H = BJ^2$ is usually corrected to introduce the centrifugal distortion correction, giving the energy levels and transition frequencies as follows:

$$E = BJ(J+1) - DJ^2(J+1)^2 + HJ^3(J+1)^3 \quad (11)$$

$$\nu = 2B(J+1) - 4D(J+1)^3 + H(J+1)^3[(J+2)^2 - J^2] + \dots \quad (12)$$

J : Rotational angular momentum. B , D , H : rotational constants.

- **Symmetric rotor in $^3\Sigma$ electronic state**:

$$H = B \cdot N^2 + \alpha N \cdot S + \frac{2}{3}\beta(3S_z^2 - S^2) \quad (13)$$

S : Electronic spin operator.

N : orbital + rotational angular momentum

B , α , β : rotational constants.

- **Asymmetric rotors**: We use the Watson-type Hamiltonian (Watson^[16], 1967) according to the notation appearing in Camy-Peyret and Flaud^[17] (1976).

A. Transition probability

The way we parametrize it is the following: $|\langle J, \tau | \mu | J', \tau' \rangle|^2 = \mu_g^2 \lambda_g(J, \tau, J^{prime}, \tau')$. J, J' represent rotational quantum numbers, τ, τ' are other quantum numbers, μ_g is the value of the dipole moment (electric or magnetic), and $\lambda_g(J, \tau, J', \tau')$ is a dimensionless parameter called oscillator strength of the particular transition.

B. Partition function

The case of symmetric linear or diatomic molecules ($^{16}\text{O}_2$), N_2O [linear] or CO) and the general asymmetric rotors must be treated individually. In the first case the energy levels are $\sim hBJ(J+1)$ where B is the rotational constant of the molecule in the considered vibrational state. There are corrections to this simple rigid rotor expression already explained (see equations 11 and 12) but for CO , the parameter D is five orders of magnitude smaller than B and for other important atmospheric molecules the ratio B/D is even larger. So, if the molecule is heteronuclear and has no nuclear spin, the degeneracy of the rotational levels (represented by the quantum number J) is $2J+1$ and we can write:

$$Q_r \simeq \sum_J (2J+1) \exp\left[\frac{-hBJ(J+1)}{KT}\right] \quad (14)$$

For the considered atmospheric temperature range it is convenient to use the expansion series of Herzberg^[18] (1950):

$$Q_r = \frac{kT}{hB} + \frac{1}{3} + \frac{1}{15} \frac{hB}{kT} + \frac{4}{315} (hB/KT)^2 + \dots \quad (15)$$

The number of terms to be considered in this expansion depends on the ratio of kT/hB . For example, for CO and a temperature of 250 K: $\frac{kT}{hB} = 90.42$ and this value is even larger for N_2O and other linear or diatomic molecules in the atmosphere. The approximation of taking the first term of this series is good within $\sim 0.4\%$ and it has been adopted in our code. However, the real partition function for $^{16}\text{O}_2$ is not kT/hB (as it is for $^{16}\text{O}^{18}\text{O}$) because this molecule has a center of symmetry. The factor $2J+1$ in 14 has to be changed by $\eta(J)[2J+1]$, $\eta(J)$ being 0 if J is even and 1 if J is odd. In that case the approximation for the partition function is: $Q_r = \frac{3kT}{2hB}$, the factor 3 coming from the spin degeneracy.

In the case of asymmetric rotors (O_3 , SO_2 ,...) there are three main rotational constants (A, B, C) in the Hamiltonian related with the three principal axes. There are also corrections due to centrifugal and other effects. Herzberg^[18] (1950) also found an approximation for the partition function in this case the validity of which is equivalent to the one we have seen for linear or diatomic molecules. It is:

$$Q_r = \left(\frac{\pi k^{3/2}}{\sigma}\right) \left(\frac{T^3}{ABC}\right)^{1/2} = \left(\frac{5.34 \cdot 10^6}{\sigma}\right) \left(\frac{T^3}{ABC}\right)^{1/2} \quad (16)$$

where σ is the order of the symmetry group to which the molecule belongs in the considered electronic and vibrational state (example: O_3 in the ground electronic and vibrational state is a C_{2v} molecule $\Rightarrow \sigma=2$).

C. Rotational constants

In table I we give the bibliographical sources for the rotational constants of the different molecular species needed to reproduce the atmospheric spectrum as seen from the ground (those molecules are listed in our previous work, Pardo et al.^[47], 2000). Other molecules have to be considered for limb sounding simulations and some of them are also listed in the same table. Of these molecules, $^{16}O_2$ and $H_2^{16}O$ need special attention because they determine the general shape of the tropospheric spectrum in the frequency range considered here (especially $H_2^{16}O$).

The dipole moments and hamiltonians we have used to determine the line parameters for the oxygen and water species come from the references in table I. Line broadening parameters mostly come from the HITRAN data base. A recent work (Chen et al.^[48], 2000) providing laboratory measurements of 17 new $H_2^{16}O$ (0,0,0) and (0,1,0) lines between 0.8 and 1.6 THz gives an update on the available water line frequencies. This list has been compared with our calculations with satisfactory results within current experimental accuracy.

V. COMPARISON TO MPM

The MPM models (Liebe et al.^{[5],[6]}, 1989, 1993) have been widely used by the remote sensing community during the past years. Specially for submillimeter applications, those models present several problems:

Molecular species	Reference
(*) H_2^{16}O	Matsushima et al ^[32] (1998)
(*) H_2^{18}O	Helminger and De Lucia ^[33] (1978)
H_2^{17}O	"
(*) H_2^{16}O (0,1,0)	Belov et al ^[34] (1987)
(*) HDO	De Lucia et al. ^[35] (1971)
(*) $^{16}\text{O}_2$	Zink & Mizushima ^[36] (1987)
$^{16}\text{O}_2$ v=1	"
(*) $^{16}\text{O}^{18}\text{O}$	Steinbach & Gordy ^[37] (1975)
$^{16}\text{O}^{17}\text{O}$	Gordy & Cook ^[38] (1984)
(*) $^{16}\text{O}_3$	Pickett et al ^[39] (1988)
$^{16}\text{O}_3$ (0,1,0)	"
$^{16}\text{O}_3$ (1,0,0)	Flaud et al ^[40] (1987)
$^{16}\text{O}_3$ (0,0,1)	"
$^{16}\text{O}^{16}\text{O}^{18}\text{O}$	Flaud et al ^[41] (1989)
$^{16}\text{O}^{18}\text{O}^{16}\text{O}$	"
$^{16}\text{O}^{16}\text{O}^{17}\text{O}$	Rinsland et al ^[42] (1991)
$^{16}\text{O}^{17}\text{O}^{16}\text{O}$	"
N_2O	Andreev et al ^[43] (1976)
CO	Gordy & Cook ^[38] (1984)
SO_2	Helminger & de Lucia ^[44] (1985)
SH_2	Lane et al ^[45] (1985)
NO_2	Semmoud-Monnanteuil et al ^[46] (1989)

TABLE I

ALL THE MOLECULES IN THIS TABLE ARE INCLUDED IN THE ATM MODEL. THOSE MARKED WITH AN ASTERISK APPEAR IN OUR 200 MHz RESOLUTION FOURIER TRANSFORM SPECTROSCOPY DATA AFTER A BRIEF INTEGRATION TIME (SEE PARDO ET AL^[47], 2000).

1. The dry continuum term is off by $\sim 29\%$ according to our measurements presented in Pardo et al.^[47], 2001.
2. No lines above 1 THz are included.
3. H₂O excess of absorption (pseudocontinuum) in the submillimeter range is introduced in different ways through the different versions of the model and none of those descriptions is in good agreement with submillimeter data.
4. Ozone and other minor components not included.
5. Parametrizations of the resonant absorption of water vapor and molecular oxygen rely upon a parameterization that is very hard to link to more “fundamental” parameters like oscillator strengths and energy levels. In addition, some line parameters have some problems. This is described in detail in the remaining of this section.

H.J. Liebe’s MPM models give the H₂O and O₂ resonant part of the atmospheric spectrum as follows:

$$\kappa_\nu = C \cdot \nu \sum_k S_k F_k(\nu), \quad C = 4.1907 \cdot 10^{-5} \quad (17)$$

using as input parameters the partial pressure of H₂O (p_e), that of the dry air (p_w), and the parameter $\theta = 300/T$, T being the physical temperature.

S_k (which is a “line strength”) is parametrized as follows:

$$O_2 : \quad S_k = \frac{a_{1k}}{\nu_k} p_d \theta^3 \exp[a_{2k}(1 - \theta)]$$

$$H_2O : \quad S_k = \frac{b_{1k}}{\nu_k} p_w \theta^{3.5} \exp[b_{2k}(1 - \theta)]$$

The parameters ν_k (resonance frequencies in GHz), a_{1k} , b_{1k} (Hz/Pa) and a_{2k} , b_{2k} (both dimensionless) are tabulated through a series of papers. The difference in the exponent of θ (3.5 for H₂O and 3 for O₂) comes simply from the fact that water vapor is an asymmetric top molecule and O₂ is symmetric so that the partition function of water is $\propto T^{3/2}$ (equation 16) while for oxygen 16 is $\propto T$. $F_k(\nu)$ is in general a complex line shape function like \mathcal{F} (equation 28 or 29) but normalized in a different way. Its imaginary part relates with our line-shape function $f(\nu, \nu_{l \rightarrow u})$ (equations 21 and 22) as follows: $F_k(\nu, \nu_{l \rightarrow u}) = \pi \nu_{l \rightarrow u} f(\nu, \nu_{l \rightarrow u})$.

Since Liebe makes his calculations in terms of refractivity, it is only the imaginary part of his function that has to be compared to our absorption formulation (eq. 10). For this comparison it is beneficial to make the following approximation (valid only at low frequencies): $e^{-E_0/KT} - e^{-E_1/KT} = e^{-E_0/KT}[1 - e^{-h\nu_k/KT}] \simeq \frac{h\nu_k}{kT} e^{-E_0/KT}$, since it appears to be the basis of Liebe's parameterization. Eliminating elements that are repeated in both cases we have (note that $\nu_{l \rightarrow u} \equiv \nu_k$):

$$\begin{aligned} \text{O}_2: \quad C \cdot a_{1k} p_d \theta^3 e^{a_{2k}(1-\theta)} &= \frac{8\pi^2 N_{\text{O}_2} \nu_k}{3cQkT} e^{-\frac{E_0}{kT}} S_k \mu_B^2 \\ \text{H}_2\text{O}: \quad C \cdot b_{1k} p_w \theta^{3.5} e^{b_{2k}(1-\theta)} &= \frac{8\pi^2 N_{\text{H}_2\text{O}} \nu_k g_k}{3cQkT} e^{-\frac{E_0}{kT}} g_k S_k \mu^2 \end{aligned} \quad (18)$$

Other elements in equations 18 that we can explicitly give are here:

O ₂	H ₂ O
$p_{\text{O}_2} = 0.2097 p_d = N_{\text{O}_2} kT$	$p_{\text{H}_2\text{O}} = N_{\text{H}_2\text{O}} kT$
$Q = \frac{3kT}{2hB}$	$Q = \left(\frac{5.34 \cdot 10^6}{\sigma[=2]}\right) \left(\frac{T^3}{ABC}\right)^{1/2}$
	$A = 835839.876 \text{ MHz}$
$B = 43100.430 \text{ MHz}$	$B = 435346.811 \text{ MHz}$
	$C = 278140.481 \text{ MHz}$
$\mu_B = 2\mu_{\text{Bohr}} = 1.854 \cdot 10^{-23} \text{ esu} \cdot \text{m}$	$\mu_B = 2\mu_{\text{Bohr}} = 1.854 \cdot 10^{-23} \text{ esu} \cdot \text{m}$

Introducing all of the above into the relations 18 we finally arrive at:

$$\begin{aligned} \text{O}_2 : \nu_k (\text{GHz}) S_k e^{-E_0/KT} &= \\ &= 24.717 a_{1k} (\text{Hz}/\text{Pa}) \exp(a_{2k}) e^{-a_{2k}/kT} \end{aligned} \quad (19)$$

$$\begin{aligned} \text{H}_2\text{O} : b_{1k} (\text{Hz}/\text{Pa}) e^{b_{2k}} e^{-b_{2k}/kT} &= \\ &= 2358.852 \nu_k (\text{GHz}) S_k g_k e^{-E_0/KT} \end{aligned} \quad (20)$$

From this it follows:

1. $a_{2k}(\text{no units}) = E_0(\text{Kelvin})/300$
2. $\frac{\nu_k(\text{GHz})S_k}{a_{1k}(\text{Hz/Pa})\exp(a_{2k})} = 24.717$
3. $b_{2k}(\text{no units}) = E_{0k}(\text{Kelvin})/300$
4. $\frac{b_{1k}(\text{Hz/Pa})\exp(b_{2k})}{\nu_k(\text{GHz})S_k g_k} = 2358.852$

For the spin-rotation O₂ lines around 60 GHz (2.) is valid within 0.2%. For the H₂O resonance at $\nu_k = 325.1529$ GHz: $g_k = 1$, $\lambda_k = 0.091$ and Liebe gives for the same resonance: $b_{1k} = 14990$, and $b_{2k} = 1.540$, so that the relation (4) above is also true within 0.2%. However, all four identities rely upon the validity of the approximation $1 - e^{-h\nu_k/KT} \simeq \frac{h\nu}{kT}$ so that the parameters a_{1k} , a_{2k} , b_{1k} and b_{2k} are somehow corrected for higher frequency resonances. Such an artifice is not necessary in our case. In addition, for the 22.24 GHz and 183.31 GHz resonances Liebe gives experimental values that make ratio (4) above fail by 7 %.

VI. LINE SHAPES

A. Absorption

In this section we deal only with the function $f(\nu, \nu_{l \rightarrow u})$ as it appears in equation 10.

In the microwave domain, the natural line width (related to the spontaneous emission lifetime) is of the order of 10^{-6} Hz and is completely negligible when compared with other broadening mechanisms taking place in the atmosphere.

In the lower atmospheric layers (up to ~ 50 km, depending on the molecule and the criteria) the collisional broadening mechanism (also called pressure-broadening) dominates the line shape. The proximity of other molecules introduces perturbations in the Hamiltonian of the molecule under study. Thus, the position of its energy levels changes and so the frequencies of different transitions are affected. The most general description of the collisional shape of lines and bands of overlapping lines has been given by Fano^[19] (1963). One approximation considers that the time between collisions, τ_{col} ($\propto P^{-1}$), is much shorter than the time for spontaneous emission, τ_{rad} , which is, in the case of a two level system, $1/A_{u \rightarrow l}$ where $A_{u \rightarrow l}$ is the Einstein's coefficient for spontaneous emission. This approximation leads to the so-called Van Vleck - Weisskopf^[20] (1945) [VWV] profile,

normalized as follows to be included in equation 10:

$$f_{VW}(\nu, \nu_{l \rightarrow u}) = \frac{\nu \Delta \nu}{\pi \nu_{l \rightarrow u}} \left(\frac{1}{(\Delta \nu)^2 + (\nu - \nu_{l \rightarrow u})^2} + \frac{1}{(\Delta \nu)^2 + (\nu + \nu_{l \rightarrow u})^2} \right) \quad (21)$$

A different approximation, leading to the kinetic line shape (Zhevakin and Naumov^[21], 1963), considers the case in which τ_{col} is much longer than τ_{rad} . The line profile is then:

$$f_{ZN}(\nu, \nu_{l \rightarrow u}) = \frac{2\nu_{l \rightarrow u} \nu \Delta \nu}{\pi(\nu_{l \rightarrow u}^2 - \nu^2)^2 + 4\nu^2 \Delta \nu^2} \quad (22)$$

For most trace atmospheric molecules, the pressure-broadening parameter $\Delta \nu$ is of the order of 2 to 3 MHz/mb (see, for example, Bouazza et al^[22], 1993, for O₃). In the impact approximation the collisional broadening parameter is of the order of $1/2\pi\tau_c$. This approximation proves to work quite well within a given distance of the resonances. For example, all the mm/submm resonances of H₂O and other molecules up to 1.2 THz are well reproduced using this approximation within that frequency range (see Pardo et al^[47], 2001). However, H₂O resonances located at higher frequencies introduce some far-wing absorption below 1.2 THz that is not equal to what is predicted from those lines simply using a VW profile. This may be due to the finite collision time. Due to the complexity of the calculations and the lack of precise laboratory data it has been simpler to add a pseudocontinuum opacity at millimeter and submillimeter wavelengths to account for this excess of absorption (see section VII). The broadening parameter also depends on the velocities of particles, i.e. it depends on temperature. This dependence will be ultimately controlled by the type of intermolecular potential. A classic type of interaction in the atmosphere is the one between an asymmetric top molecule (C_{2v} group, for example H₂O or O₃) and a linear molecule (O₂ and N₂). The potential can be written as a sum of the molecular electrostatic contributions and atom-atom contributions (Labani et al^[23], 1986). For laboratory measurements of the collisional broadening parameter and its temperature dependence, the following expression is usually adopted (Barbe et al^[24], 1996):

$$\Delta \nu(P, T) = \Delta \nu(P_0, T_0) \frac{P}{P_0} \left(\frac{T_0}{T} \right)^\gamma \quad (23)$$

Laboratory measurements provide $\Delta\nu(P_0, T_0)$ and γ and the results are tabulated in the spectroscopic data bases.

In the atmosphere we neglect the effect of self-collisions of trace gases (for example, for O_3 we neglect O_3-O_3) and we consider collisions of only two types: self collisions of abundant molecules (O_2 and H_2O) and collisions involving all species with one of the two main atmospheric components (O_2 and N_2). From the works of Connor et al^[25] (1986), Gamache et al^[26] (1985) and Bouazza et al^[22] (1993), and others, the following “additional” law for the collisional broadening parameters of molecule M is suggested:

$$\Delta\nu(M - dry\ air) = X_{N_2}\Delta\nu(M - N_2) + X_{O_2}\Delta\nu(M - O_2) \quad (24)$$

where X are the volume mixing ratios. The P and T dependence is implicit. Laboratory measurements for individual lines are the only source of precise information about the parameters γ and $\Delta\nu(M - N_2)$ for the different atmospheric trace gases. The exponent γ has been found in most cases to be in the range 0.6 and 1.0. Thus, taking into account the range of atmospheric temperatures and pressures that we are considering it is clear that the well known linear pressure dependence plays a much more important role than the temperature exponent γ on the collisional width. This is the reason limb sounding systems use the linewidths to establish the pressure (vertical) grid (see Fishbein et al^[27], 1996).

The only atmospheric molecule other than O_2 for which self-collisions have to be considered in the context of resonance lines is H_2O . Such self-collisions play an important role on the shape of the strong atmospheric resonances of this molecule in the lower troposphere. For self collisions the temperature exponent is 1. However, for the high altitude sites considered below, this term is negligible.

When the pressure gets very low the Doppler effect due to the random thermal molecular motion dominates the line broadening. If we calculate the distribution of frequencies close to a molecular resonance from a sample of molecules whose velocities are described by a Maxwellian distribution, one obtains a Gaussian line shape, which we normalize as follows to be compatible with expression 8:

$$\mathcal{F}_D(\nu, \nu_{l \rightarrow u}) = \frac{1}{\Delta\nu_D} \left(\frac{\ln 2}{\pi} \right)^{1/2} \exp \left[- \left(\frac{\nu - \nu_{l \rightarrow u}}{\Delta\nu_D} \right)^2 \ln 2 \right] \quad (25)$$

where the halfwidth parameter is given by:

$$\Delta\nu_D = \frac{\nu_{l \rightarrow u}}{c} \sqrt{\frac{2 \ln 2 k T}{m}} = 3.58 \cdot 10^{-7} \nu_{l \rightarrow u} \sqrt{\frac{T}{M}} \quad (26)$$

M being the molecular weight of the species in g/mol.

If the collisional and thermal broadening mechanisms are comparable the resulting line-shape is the convolution of a Lorentzian (collisional line shape at low pressures) with a Gaussian, generally called Voigt profile:

$$\mathcal{F}_V(\nu, \nu_{l \rightarrow u}) = \int_{-\infty}^{\infty} \mathcal{F}_L(\nu, \nu') \mathcal{F}_D(\nu', \nu_{l \rightarrow u}) d\nu' \quad (27)$$

B. Phase delay

Besides absorption, the propagation through the atmosphere also introduces a phase delay. This phase delay increases as the wavelength approaches a molecular resonance, with a sign change across the resonance. The process can be understood as a forward scattering by the molecular medium in which the phase of the radiation changes.

Both the absorption coefficient and the phase delay can be treated in a unified way for any system since both parameters are derived from a more fundamental property, the complex dielectric constant, by means of the Kramers-Krönig^{[28],[29]} relations. Application of the Kramers-Krönig theory to evaluate phase dispersion allows our model to make predictions for future submm interferometry sites.

A generalized (complex) expression of the VVW profile, which accounts for both the Kramers-Krönig^{[28],[29]} (1926) dispersion theory as well as line overlapping effects (parameter δ , see Rosenkranz^[30], 1988) is the following ($\nu_{l \rightarrow u} \equiv \nu_{lu}$):

$$\mathcal{F}_{VVW}(\nu, \nu_{lu}) = \frac{\nu}{\pi \nu_{lu}} \left[\frac{1 - i\delta}{\nu_{lu} - \nu - i\Delta\nu} + \frac{1 + i\delta}{\nu_{lu} + \nu + i\Delta\nu} \right] \quad (28)$$

the imaginary part of which reduces to equation 21 when $\delta=0$.

The complex expression of the kinetic line profile (Gross^[31], 1955) is:

$$\mathcal{F}_G(\nu, \nu_{l \rightarrow u}) = \frac{2\nu_{l \rightarrow u} \cdot (\nu_{l \rightarrow u}^2 - \nu^2 + i\nu\Delta\nu)}{\pi(\nu_{l \rightarrow u}^2 - \nu^2)^2 + 4\nu^2\Delta\nu^2} \quad (29)$$

VII. NON-RESONANT ABSORPTION

A. Review of the H_2O pseudocontinuum

Since we include lines with resonant frequencies only up to 10 THz and the true line-shape is not known accurately, a broadband “continuum”-like absorption term needs to be included (e.g. Clough et al^[49], 1989; Waters^[50], 1976). If the far wings are not well reproduced by an assumed collisional line shape or too few lines are included in the summation, a residual (negative or positive) opacity remains. For example, as explained in section VI-A failure of the impact-approximation line-shape is expected below 1.2 THz for the far H_2O line wings of those resonances centered above 1.2 THz. The earliest attempt to introduce an empirical continuum correction at millimeter wavelengths was done by Gaut and Reifenstein^[51] (1971). Measurements of this absorption in the millimeter domain were first performed by Rice et al^[52] (1979). Ma and Tipping^[53] (1990) performed a rigorous study of the water vapor “self-broadened” pseudo-continuum term (involving binary collisions of water molecules) at millimeter and submillimeter wavelengths, but not of foreign gas broadening, likely the dominant effect at high altitudes. Clough et al^[49] define a “foreign” pseudo-continuum absorption (for collisions of H_2O with either O_2 or N_2) by considering far wings ($|\nu - \nu_i| \geq 25 \text{ cm}^{-1}$) of all water vapor lines from 0 to 10000 cm^{-1} and making a semiempirical correction to the line-shape for the impact approximation.

B. Dry continuum-like absorption

The non resonant absorption of the dry atmosphere is made up of two components: collision induced absorption due to transient electric dipole moments generated during binary interactions of symmetric molecules with electric quadrupole moments such as N_2 and O_2 , and the relaxation (Debye) absorption of O_2 . The physical explanation of the second term is the following: in the presence of incident radiation of frequency ν the oxygen molecule can absorb energy from the magnetic field \vec{H} of the wave and its permanent magnetic dipole $\vec{\mu}_{O_2}$ is oriented according to a Boltzmann distribution determined by the factor $\exp[-\vec{\mu}_{O_2} \vec{H}/KT]$. This absorption appears with no particular resonance frequency

(except zero) and has the following expression (Debye^[54], 1929):

$$(\kappa_\nu)_{Debye} = \frac{16\pi^2 N |\mu|^2}{3ckT} \frac{\Delta\nu}{1 + \left(\frac{\Delta\nu}{\nu}\right)^2} \quad (30)$$

where $\Delta\nu$ is now the relaxation frequency (see below) above which the dipoles can no longer follow the field. For O_2 in the atmosphere this absorption has to be taken into account at least below 100 GHz (Rosenkranz^[55], 1993). The Debye spectrum of O_2 is introduced according to equation 30 with the relaxation frequency, directly related to the mean lifetime between collisions, equal to $0.05369 \cdot PT^{-0.8}$ GHz (Liebe et al^[6], 1993).

C. Pseudocontinua in ATM

In our ATM model, we introduce collisionally-induced dry absorption and longwave (foreign) pseudocontinuum water vapor absorption derived from our previous FTS measurements performed on top of Mauna Kea, Hawaii. For both terms we use ν^2 frequency power laws, with the coefficients as determined by Pardo et al^[47], 2001.

$$\kappa_{c,H_2O} = 0.031 \cdot \left(\frac{\nu}{225}\right)^2 \cdot \left[\frac{e}{1013} \cdot \frac{P-e}{1013}\right] \cdot \left(\frac{300}{T}\right)^3 m^{-1} \quad (31)$$

$$\kappa_{c,dry} = 0.0114 \left(\frac{P-e}{1013}\right)^2 \left(\frac{300}{T}\right)^{3.5} \left(\frac{\nu}{225}\right)^2 m^{-1} \quad (32)$$

For details about these expressions see the above reference. We are continuing to collect data under various atmospheric (humidity) conditions and so the coefficients will no doubt be refined somewhat in the future. The validity of these expressions is restricted to frequencies ≤ 1.1 THz (the upper limit of our current data. Above 1.1 THz it is better to use the N_2 - N_2 continuum formulation of Borysow and Frommhold^[56] (1986) (far-infrared collision-induced spectrum of nitrogen) scaled upward by a factor of 1.29. The 29% correction has been found necessary to fit our FTS data (Pardo et al^[47], 2001) and accounts for additional collisional mechanisms such as N_2 - O_2 and O_2 - O_2 collisions, etc... The simple ν^2 law used above loses validity beyond ~ 1 THz as the center of the band (at $\nu \simeq 2.4$ THz) is approached. The validity of this assumption will be tested with further FTS measurements extending to higher frequencies.

VIII. EXPERIMENTAL BASIS

As described above, a series of FTS measurements on Mauna Kea are providing a data set against which we are testing and refining the model. Some results obtained during extremely dry conditions allowed us to separately measure for the first time the submillimeter wet and dry pseudocontinua terms (Pardo et al. 2000). After revising the model to take those results into account and everything detailed in this paper, our new FTS data obtained during the past year are fitted extremely well. As an example we present here two measurements obtained in March and July 2000 and their corresponding fits (figure 1). When completed, the whole data set will be presented in a future paper, along with our final best-fit coefficients for the pseudocontinuum terms.

IX. PREDICTIONS FOR SUBMILLIMETER SITES

During the past few years, new ground-based astronomical observatories have been built to allow access to the submillimeter range of the electromagnetic spectrum. Potential sites are now being tested for more ambitious instruments such as the *Atacama Large Millimeter Array* (ALMA). All of these are remote, high altitude sites. For our simulations we have selected three sites of interest for submillimeter astronomy: Mauna Kea, HI, USA (LAT=19:46:36, LONG=-155:28:18; home of the Caltech Submillimeter Observatory, James Clerk Maxwell Telescope and Submillimeter Array), Chajnantor, Chile (LAT=-23:06, LONG=-67:27; site selected for ALMA) and the Geographic South Pole (site of the Antarctic Submillimeter Telescope and Remote Observatory).

To analyze the differences between these sites we have run our best-fit ATM model for typical T/P profiles obtained from in-situ radiosonde measurements and compare predictions for the same zenith precipitable water vapor columns (N_{H_2O} , in mm). We have used 0.15, 0.5 and 1.0 mm of water to reproduce conditions ranging from outstanding to good zenith submillimeter submillimeter transmission. Of course, the percentage of time for which the integrated column of water vapor is below a given value is different for each site and that can also contribute to making one site superior to another. Here we will not discuss opacity statistics of the different sites, but rather focus on the differences for a given, common amount of water vapor. The T/P profiles used in the simulations have

been obtained from:

- Mauna Kea site (MK): Radiosoundings launched twice daily from the nearby Hilo airport (~ 25 miles away), truncated on the lower end at 4.1 km. The T/P profile considered here is the average for the period Nov. 1st, 1999 - Jan. 31th, 2000 (winter).
- Chajnantor (CH): The Chajnantor radiosonde campaign is a collaboration between the National Radio Astronomy Observatory, the European Southern Observatory, Cornell University, the Smithsonian Astrophysical Observatory, and the Japanese LMSA project. The T/P profile considered here is the average (from 28 radiosoundings) corresponding to the Nov. 1999 campaign (summer).
- Geographic South Pole (SP). The radiosonde T/P profiles used here come from in situ winter-time measurements provided by R. Chamberlin (from Chamberlin and Bally^[57], 1995).

The three profiles we have used are plotted on figure 2. Although the MK and CH profiles correspond to different seasons they are fairly similar except for the starting altitude/pressure. We know that on Mauna Kea, the night-time ground-level temperatures typically fall within the range 273 ± 5 K year round, and the same seems to apply to Chajnantor. The SP site is much colder and also lower.

We first compare the transmission for the three sites under the same water vapor column. We begin with the 0.15 mm case, an outstanding situation for ground based submillimeter-wave astronomy. Such a low water vapor column seems to be a lower limit for all three sites considered here. FTS data have already shown water vapor columns very close to that value [Pardo et al^[47] (2001), Matsushita et al^[58] (1999) and Paine et al^[59] (2000)]. At the South Pole, the cold winter temperatures and the saturation of water vapor indicate that such conditions would happen quite often at this site (note that $N_{H_2O}=0.5$ mm gives an oversaturation for SP winter over an important vertical range). The comparison of the calculated atmospheric transmissions for this case is shown in Figure 3.

It may seem surprising from this figure that the worst transmission is predicted for the case of the South Pole Site. This result arises from the combination of several factors:

- A) The higher ground level pressure and the lower temperature both make the resonant

absorption broader (equation 23).

B) The dry continuum (middle panel of Figure 3) and H_2O pseudocontinuum (bottom panel of Figure 3) terms are both higher due to the higher pressures as well (eqs. 31 and 32).

C) The partition function is a positive temperature power law (see e.g. equation 16), causing absorption in low energy levels to increase as temperature decreases.

Under equal water vapor column conditions, the transmission in the high frequency atmospheric windows (above 550 GHz) is then nearly a factor of two lower at SP than at CH, while MK is only about 10% worse than CH. In other words, the transmissions at the CH and SP sites would be similar if CH had twice the water vapor column of the SP site. This does not automatically mean that Chajnantor is a superior site to the South Pole, because the frequency distribution of N_{H_2O} also needs to be taken into account. This suggests that to evaluate sites, T/P data need to be weighted by N_{H_2O} statistics, or better yet, direct transmission measurements should be compared. Here we have taken N_{H_2O} cumulative distributions from Lane et al.^[60] (1998) and have performed a direct comparison of the three 25% quartile for each site in winter (Figure 4). The South Pole distributions are derived from radiosonde flights and are probably optimistic respect to those of the other two sites that were derived from radiometric 225 GHz data.

A. Atmospheric phase delay

Another issue of importance primarily for interferometry, is the atmospheric phase delay. Present day radio interferometers are mostly limited to frequencies below 350 GHz. Phase delay increases in importance as the frequency increases into the submillimeter domain because of the strength of the atmospheric lines involved in both absorption and dispersion. Using the complex line shape of equation 28 we have calculated the derivative of the phase delay respect to the water vapor column $\frac{\partial \phi}{\partial N_{H_2O}}$ (this derivative will be called the *differential phase* and is provided in deg/ μm here). The differential phase as a function of frequency has been plotted for the Chajnantor site in figure 5 (where the curve is restricted to those frequencies where the transmission is above 10% when the precipitable water vapor column is 0.3 mm, i.e. very good conditions for single-dish submillimeter observations). Another useful quantity plotted in the same figure is the derivate of the phase delay with respect

to the sky brightness temperature ($T_{B,sky}$), since this function relates the phase correction between two antennas to a measurable physical parameter ($T_{B,sky}$). Note however that whereas the differential phase described above depends only on ΔN_{H_2O} , this new quantity depends on the absolute H_2O column as well. The curve plotted here corresponds to $\frac{\partial \phi}{\partial T_b}(\nu)$ at $N_{H_2O}=0.3\text{mm}$. On the same figure we plot the curves $\frac{\partial T_b(\nu)}{\partial N_{H_2O}}$ around the water vapor lines at 22.23, 183.31, and 325.15 GHz also for $N_{H_2O}=0.3\text{ mm}$. Of these, the lines at 183.31 and 325.15 GHz are the best choices to monitor water vapor path differences between antennas for differential phase corrections in the range of water vapor columns that allow submillimeter observations to be carried out. The reason for this is that the center of these lines displays a brightness temperature range of $\sim 170\text{ K}$ for water vapor columns between 0.15 and 1.5 mm (for larger H_2O columns transmission at the center of the 650 and 850 GHz atmospheric windows falls below 15 %), a range that is unmatched by any other water vapor line below 1 THz.

As seen in figure 5, the differential phase becomes much more important in the sub-millimeter domain than it is at millimeter wavelengths, so its correct estimation and the selection of the best means of monitoring water vapor column differences between different antennas are essential for ground-based submillimeter interferometry. For example, the differential phase is $0.0339\text{ deg}/\mu\text{m}$ at 230 GHz whereas it is -0.4665 and $0.2597\text{ deg}/\mu\text{m}$ at 650 and 850 GHz respectively, roughly an order of magnitude larger.

B. Atmospheric spectrum for SOFIA

Finally, we have performed one further simulation of the zenith atmospheric. This one is for the 1-4000 GHz range above 13.2 km, the operating altitude of the future Stratospheric Observatory for Infrared Astronomy (SOFIA, see Becklin^[61], 1997) shown in Figure 6. The SOFIA sky spectrum is mainly dominated by ozone, H_2O and O_2 lines, but there is also a small dry continuum (modeled after Borysow and Frommhold^[56], 1986 with the 29 % correction given in section VII-C, responsible for about 4% absorption at 3 THz. On the other hand, the H_2O pseudocontinuum at this altitude is negligible.

X. SUMMARY AND CONCLUSIONS

Our current atmospheric radiative transfer model, ATM, has been described in detail. It includes the absorption and phase delay effects due to all H_2O , O_2 and O_3 resonances up to 10 THz. It also includes semiempirical continuum-like terms derived from our FTS measurements on Mauna Kea. The model thus has applicability to fields as diverse as astronomy, remote sensing and communications.

Based upon our current best-fit model, it is possible to show that Chajnantor (the future site of ALMA) provides significantly better transmission than the South Pole for equal water vapor columns. In fact, below 0.5 mm of H_2O , equivalent transmissions occur at the two sites with a factor of 2 higher water vapor present at Chajnantor. This is important to fold into comparisons of the two sites.

The first simulations of phase delay have been presented here as a first step to selecting strategies for its correction in future submillimeter interferometers such as ALMA.

Other simulations have been devoted to the atmospheric transmission for the operating altitude of the SOFIA instrument showing how trace gases opacity becomes locally important and needs to be well modeled.

ACKNOWLEDGMENTS

This work is supported by U.S. NSF grants ATM-9616766 and AST-9980846, and by Spanish CICYT grants PNIE98-1351E and PB96-0883. J.R. Pardo also acknowledges partial financial support for his work from the Goddard Institute for Space Studies in New York City, *Observatoire de Paris-Meudon*, *CNES* and *Météo-France* under the *décision d'aide à la recherche 795/98/CNES/7492*.

REFERENCES

- [1] Grossman, E. *AT User's Manual*, (Airhead Software, 1609 Bluff Street, Boulder, Colo. 80302), 1989.
- [2] Cernicharo, J., *ATM: a program to compute atmospheric transmission between 0-1000 GHz*, Internal report of the *Institut de Radioastronomie Millimétrique (IRAM)*, 1985.
- [3] Cernicharo, J., Ph.D. Thesis, Université de Paris VII, 1988.
- [4] Pardo, J.R., Ph.D. Thesis, Université de Paris VI, 1996.
- [5] Liebe, H.J., *Int. J. Infrared Mill. Waves*, 1989, 10, 631-650.
- [6] Liebe, H. J., Hufford G. A., and Cotton M. G., *Proceedings of AGARD 52nd Specialists' Meeting of the Electromagnetic Wave Propagation Panel*, Palma de Mallorca (Spain), 1993.

- [7] L.S. Rothman, R.R. Gamache, R.H. Tipping, C.P. Rinsland, M.A.H. Smith, D. Chris Benner, V. Malathy Devi, J.-M. Flaud, C. Camy-Peyret, A. Perrin, A. Goldman, S.T. Massie, L.R. Brown, and R.A. Toth, J. Quant. Spectrosc. Radiat. Transfer, 1992, 48, 469-507.
- [8] H. M. Pickett, R. L. Poynter, E. A. Cohen, M. L. Delitsky, J. C. Pearson, and H. S. P. Muller, J. Quant. Spectrosc. Radiat. Transfer, 1998, 60, 883-890.
- [9] Jacquinet-Husson N., E.Arié, J.Ballard, A.Barbe, G.Bjoraker, B.Bonnet, L.R.Brown, C.Camy-Peyret, J.P.Champion, A.Chédin, A.Chursin, C.Clerbaux, G.Duxbury, J.M.Flaud, N.Fourrié, A.Fayt, G.Graner, R.Gamache, A.Goldman, Vl.Golovko, G.Guelachvili, J.M.Hartmann, J.C.Hilico, J.Hillman, G.Lefèvre, E.Lellouch, S.N.Mikhalevko, O.V.Naumenko, V.Nemtchinov, D.A.Newnham, A.Nikitin, J.Orphal, A.Perrin, D.C.Reuter, C.P.Rinsland, L.Rosenmann, L.S.Rothman, N.A.Scott, J.Selby, L.N.Sinitsa, J.M.Sirota, A.M.Smith, K.M.Smith, Vl.G.Tyuterev, R.H.Tipping, S.Urban, P.Varanasi, M. Weber, J. Quant. Spectrosc. Radiat. Transfer, 62, N2, 205-254 (1999).
- [10] Pardo, J.R., M. Gérin, L. Pagani, and C. Prigent, J. Quant. Spectrosc. Radiat. Transfer, 54, N6, 931 (1995)
- [11] Pardo, J.R., M. Gérin, C. Prigent, J. Cernicharo, G. Rochard, and P. Brunel, J. Quant. Spectrosc. Radiat. Transfer, 60, 4, 559-571 (1998).
- [12] Pardo, J.R., M. Ridal, D. Murtagh, and J. Cernicharo. Accepted, Canadian Journal of Physics [Special Odin Issue], (2000).
- [13] Pardo, J.R., M. Mishchenko, C. Prigent, and W. Rossow. In preparation, (2001).
- [14] Chandrasekhar, S., *Radiative Transfer*, Oxford University Press (1960).
- [15] Kroto, H.W., *Molecular Rotation Spectra*, John Wiley & Sons, Ltd. New York (1975).
- [16] Watson, J.K.G., J. Chem. Phys., 46, pp. 1935 (1967).
- [17] Camy-Peyret, C., and Flaud, J.M., Molecular Physics, Vol. 32, N. 2, 523-537 (1976).
- [18] Herzberg, G., *Spectra of Diatomic Molecules*, Van Nostrand Reinhold Company, (1950).
- [19] Fano, U., Phys. Rev. 131, 259 (1963).
- [20] Van Vleck JH, Weisskopf VF. Rev. Mod. Phys., 17, 227-236 (1945).
- [21] Zhevakin SA, Naumov AP. Izv. Vysshik Chebn. Zavedenii Radiofiz, 6, 674-694 (1963).
- [22] Bouazza, S. et al, J. Mol. Spectrosc., 157, 271 (1993).
- [23] Labani, B., Bonamy, J., Robert, D., Hartmann, J.M., and Taine, J., J. Chem. Phys., 84, 4256-4267 (1986).
- [24] Barbe, A., L. Regalia, J. Plateaux, P. Von der Heyden, and X. Thomas, J. Mol. Spectrosc., 180, 175-182 (1996).
- [25] Connor, B.J. et al, J. Mol. Spectrosc., 117, 15 (1986).
- [26] Gamache, R.R. et al, J. Mol. Spectrosc., 128, 283 and 360 (1985)
- [27] Fishbein, E.F., et al., J. Geophys. Res., 101, D6, 9983-10016 (1996).
- [28] Kramers H.A., Nature, 117, 775 (1926).
- [29] Krönig, R. de L., J. Opt. Soc. Am., 12, 547 (1926).
- [30] Rosenkranz P.W., J. Quant. Spect. Radiat. Transfer, 39, N. 4, 287 (1988).
- [31] Gross, EP. Phys. Rev., 97, 395-403 (1955).
- [32] Matsushima et al., J. Mol. Struc., 352/353, 371-378 (1955).
- [33] Helminger, P.A., de Lucia, J. Mol. Spectrosc., 70, 263-269 (1978).
- [34] Belov, S.P., I.n. Kozin, O.L. Polyansky, M. Yu, M. Tret'yakov and N.F Zobov, J. Mol. Spectrosc., 126, 113-117 (1987).
- [35] De Lucia, F.C., Cook, R.L., Helminger, P., and W. Gordy, J. Chem. Phys., 55, 5334 (1971).

- [36] Zink, L.R. and M. Mizushima, J. Mol. Spectrosc., 125, 154-158 (1987).
- [37] Steinbach W. and Gordy W, Phys. Rev., A11, 729-731 (1975).
- [38] Gordy, W. Cook, R.L. *Microwave Molecular Spectra*, John Wiley and Sons (1984).
- [39] Pickett et al., J. Mol. Spectrosc., 128, 151-171 (1988).
- [40] Flaud, J.M., et al., J. Mol. Spectrosc., 124, 209-217 (1987).
- [41] Flaud, J.M., et al., J. Mol. Spectrosc., 133, 217-223 (1989).
- [42] Rinsland, C.P. et al., J. Mol. Spectrosc., 149, 474-480 (1991).
- [43] Andreev A. et al., J. Mol. Spectrosc. 62, 125-148 (1976).
- [44] Helminger, P.A., de Lucia, J. Mol. Spectrosc., 111, 66-72 (1985).
- [45] Lane, W.C. et al., J. Mol. Spectrosc., 111, 320-326 (1985).
- [46] Semmoud-Monnanteuil, N. et al., J. Mol. Spectrosc., 134, 176-182 (1989).
- [47] Pardo, J.R., E. Serabyn, and J. Cernicharo, J. Quant. Spectrosc. Radiat. Transfer, 68/4, 419-433 (2001).
- [48] Chen, P., Pearson, J.C., Pickett, H.M., Matsuura, S., and G.A. Blake, 128, 371-385 (2000).
- [49] Clough, S.A., Kneizys, F.X. and Davies, R.W., Atmos. Res., 23, 229-241 (1989).
- [50] Waters, J.W., *Absorption and emission by atmospheric gases, Methods of Experimental Physics*, 12B, 142-176 (1976).
- [51] Gaut N.E. and E.C. Reifstein III, Environ. Res. and Tech. Rep. No. 13, Lexington, Massachusetts (1971).
- [52] Rice, D.P., Ade, P.A.R., Infrared Physics, 19, 575-584 (1979).
- [53] Ma, Q. and Tipping, R.H., J. Chem. Phys., 93, 6127-6139 (1990).
- [54] Debye, (1929)
- [55] Rosenkranz, P.W., *Absorption of microwaves by atmospheric gases, in Atmospheric Remote Sensing by Microwave Radiometry*, edited by M.A. Janssen, chap. 2, John Wiley and Sons Inc., (1993).
- [56] Borysow A, Frommhold L., Astrophys. J., 311, 1043-1057 (1986).
- [57] Chamberlin RA, and Bally J., Appl. Opt., 33(6), 1095 (1994).
- [58] Matsushita S, Matsuo H, Pardo J.R., Radford S., Publ. Astron. Soc. Japan, 51(5), 603-610 (1999).
- [59] Paine S, Blundell R, Papa D.C., Barrett J.W., Radford S.J.E., PASP, 112, 767, 108-118 (2000).
- [60] Lane, A.P., Submillimeter Transmission at South Pole, in Astrophysics from Antarctica, ed. Novak, G., & Landsberg, R. H., ASP Conf. Ser. 141, p 289-295 (1998).
- [61] E. E. Becklin, *Stratospheric Observatory for Infrared Astronomy (SOFIA), Proceedings of the ESA Symposium "The Far Infrared And Submillimetre Universe"* 15-17 April 1997, Grenoble, France, ESA SP-401 pp. 201-206 (August 1997).

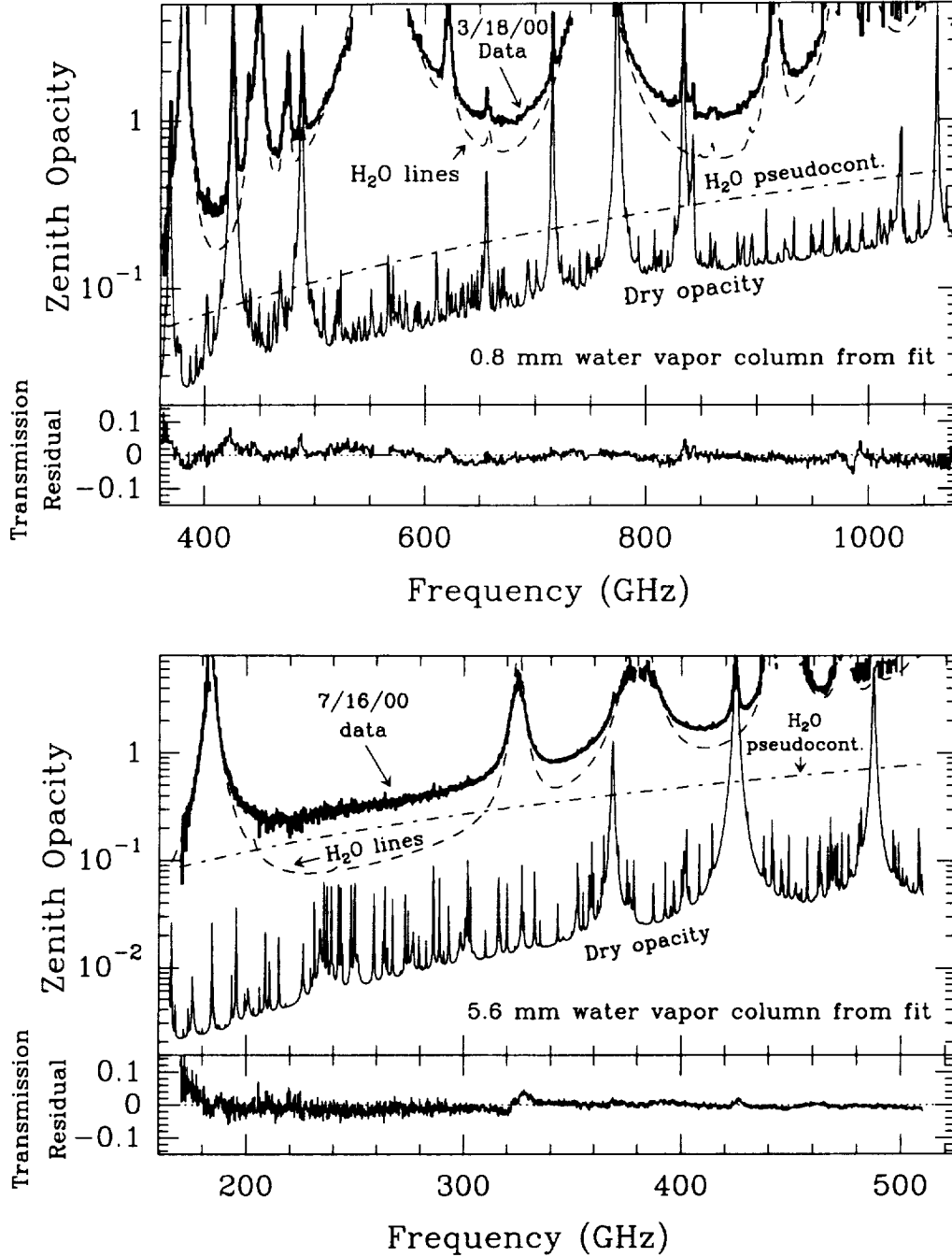


Fig. 1. FTS zenith atmospheric opacity spectra obtained on Mauna Kea in March and July 2000 and best-fit opacity contributions. The estimated water vapor columns differ by a factor of 7. Because the curve $\tau_{fit}(\nu)$ matches the data so well, the fit residuals are shown as the transmission difference ($\exp[-\tau_{meas}] - \exp[-\tau_{fit}]$). The fitting routine that produced these results is based on the radiative transfer code described in this paper, and uses only the precipitable water vapor column as a free parameter (P/T profile is fixed from the readings of the Mauna Kea weather station, our own hand-held thermo/hygrometer and Hilo airport radiosoundings).

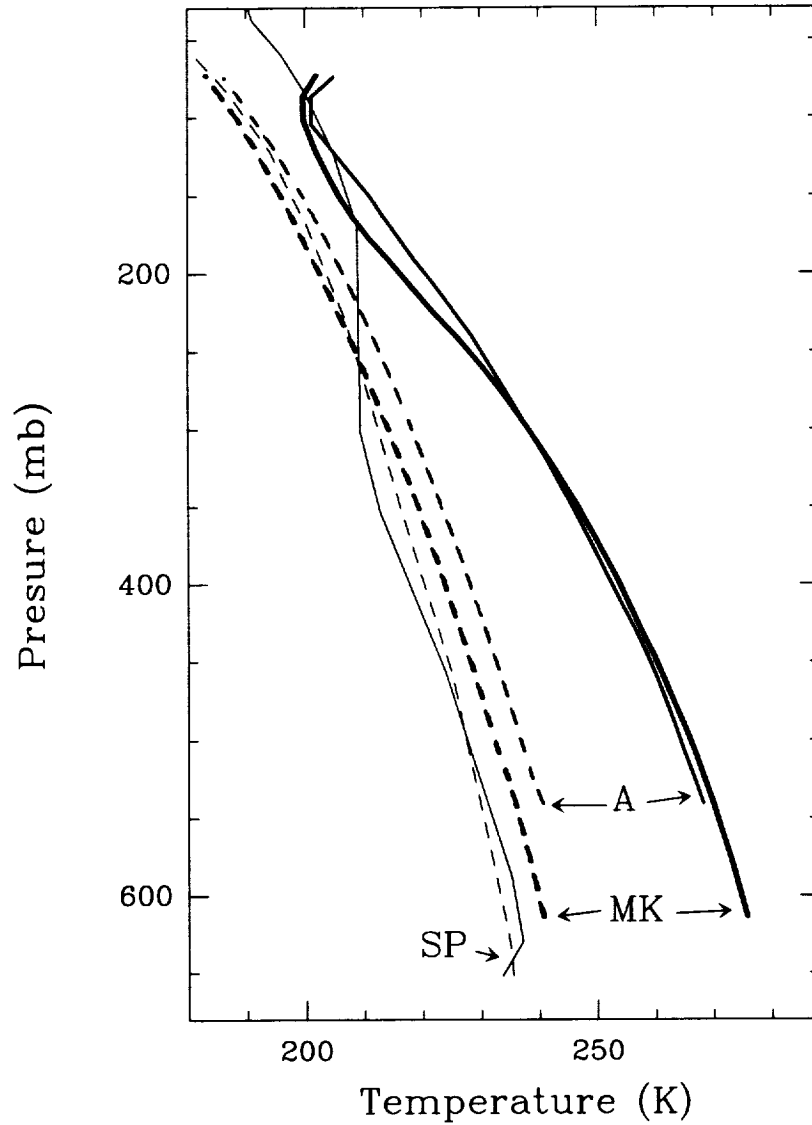


Fig. 2. Atmospheric T/P profiles (solid lines) for the three sites considered in our calculations (see text).

In order to make a comparison of the different sites under the same columns of water vapor, we have introduced moisture profiles with a total of 0.15, 0.5 and 1.0 mm for each site. In the figure we show the dewpoint temperatures (dashed lines) that correspond to 0.5 mm of water vapor column above each site. Note that the moisture would be above saturation for the South Pole Winter profile in that case (below saturation for 0.15 mm).

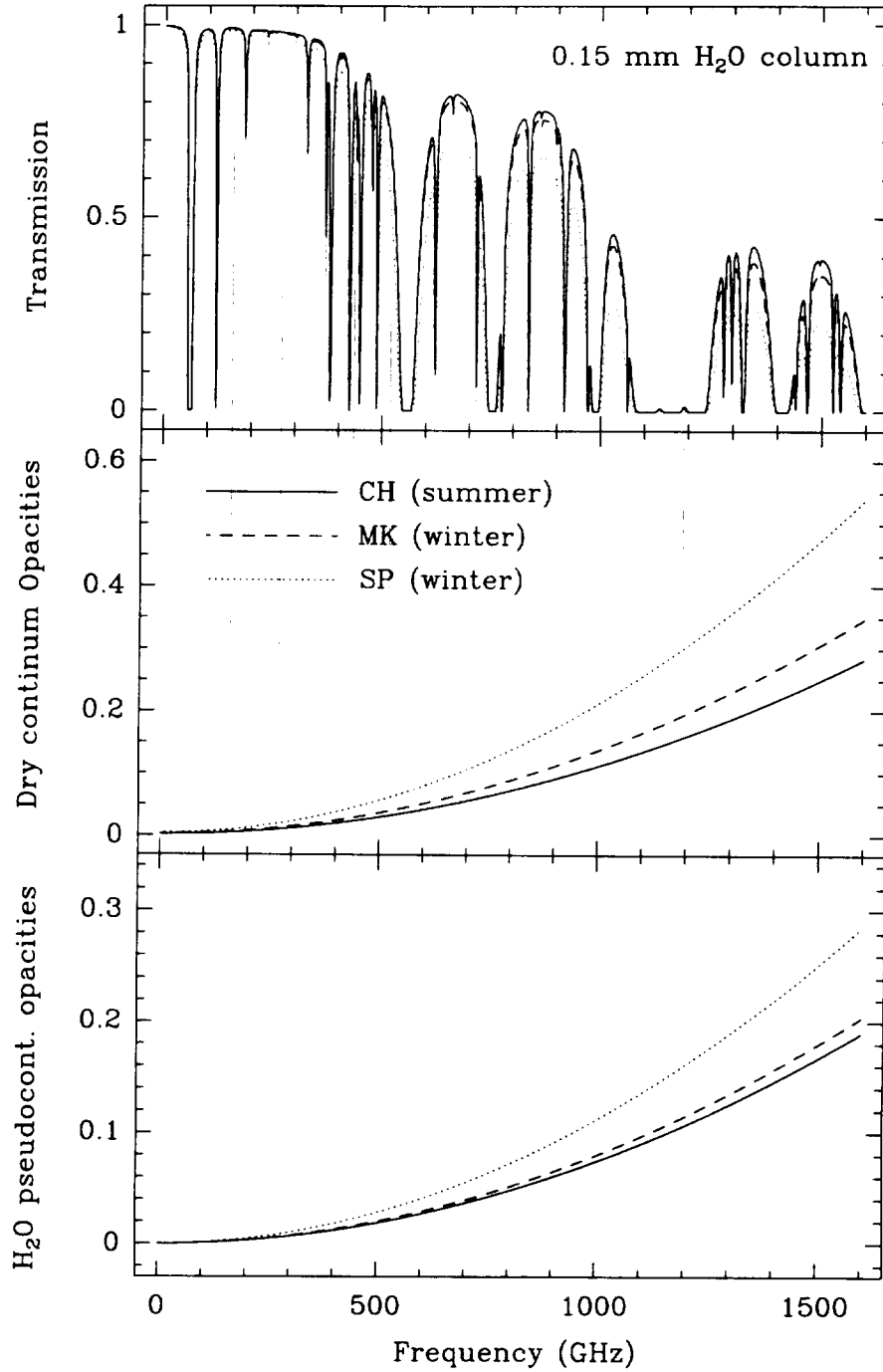


Fig. 3. Calculated atmospheric transmissions and continuum-like opacities for the three atmospheric profiles of Figure 2. Solid, dashed and dotted line indications apply also for the upper panel. Minor gases have been removed for clarity.

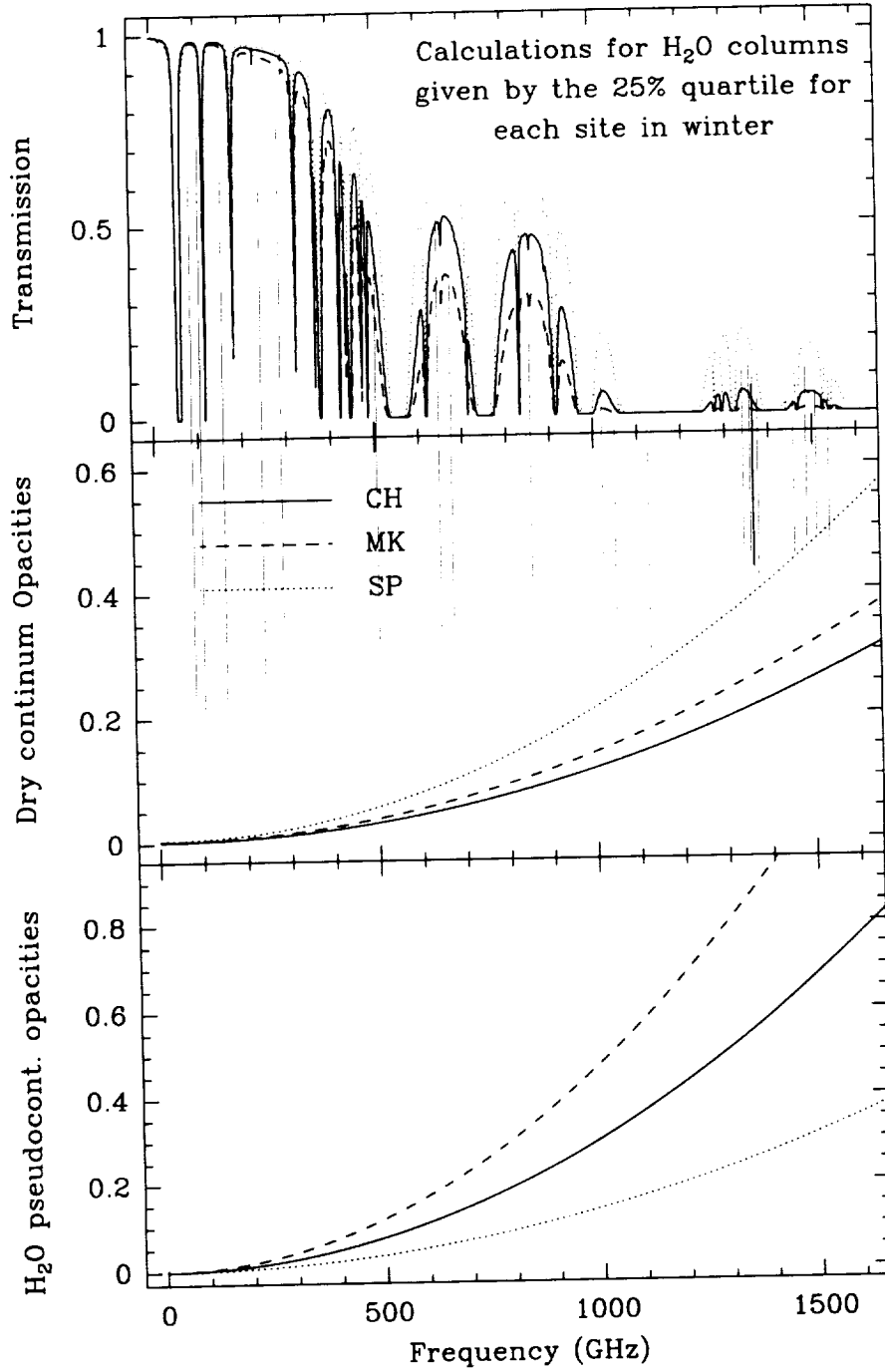


Fig. 4. Calculated atmospheric transmissions and continuum-like opacities for the three atmospheric T/P profiles of Figure 2 but considering now N_{H_2O} amount at the 25% quartile of the cumulative N_{H_2O} function for winter time in the three sites. Minor gases have been removed for clarity. Solid, dashed and dotted line indications as in figure 3. As indicated in the text, the distributions used here were derived from different methods leading probably to a comparative optimistic result for the South Pole.

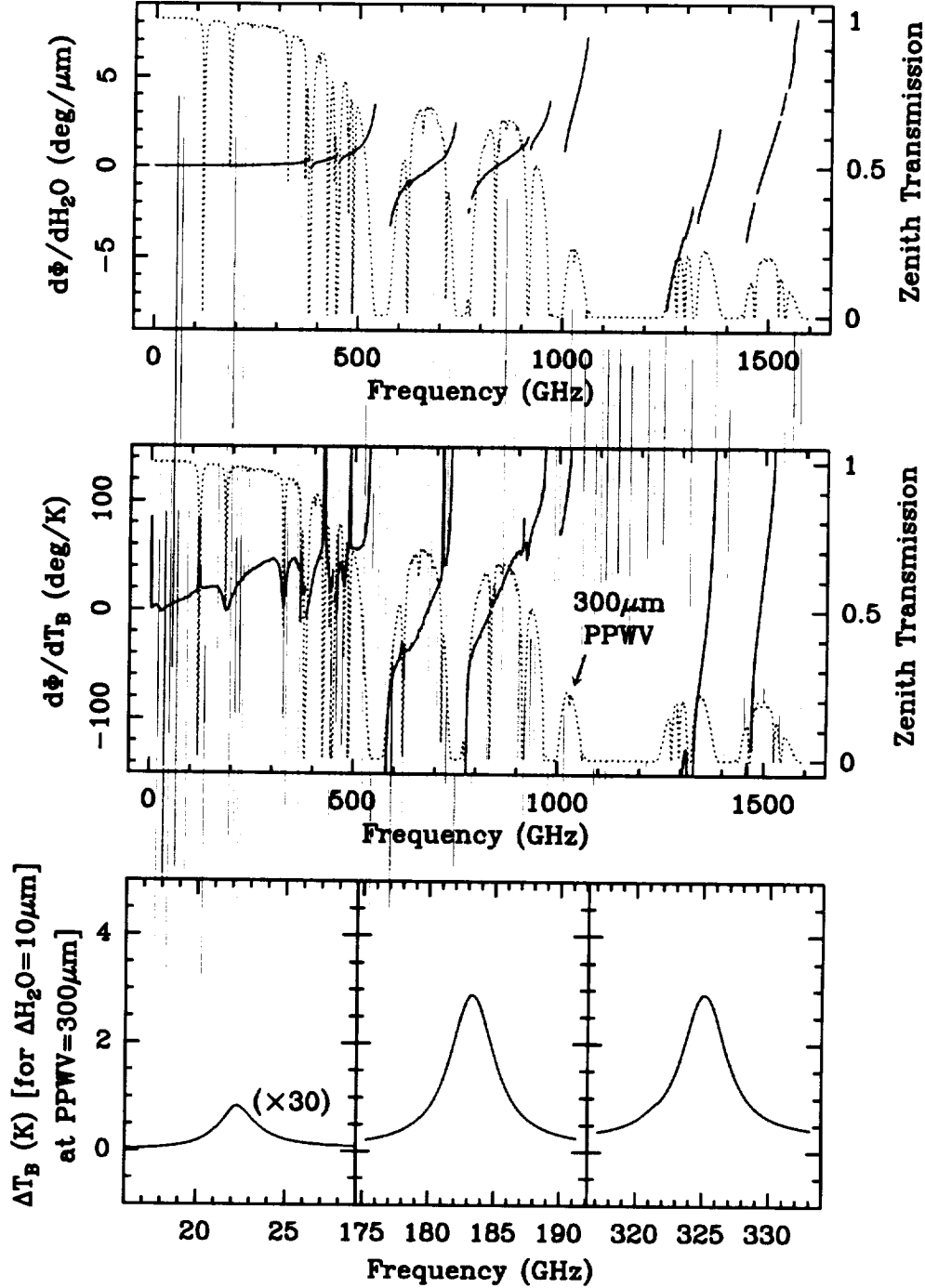


Fig. 5. Upper panel: Derivative of the phase delay respect to the water vapor column (*differential phase* in text; this derivative is independent of the water vapor column) as a function of frequency, superposed on the Chajnantor atmospheric transmission curve for 0.3 mm of water vapor. Middle panel: Derivative of the phase delay respect to the sky brightness temperature for 0.3 mm H_2O column. Lower panel: $\left[\frac{\partial T_b(\nu)}{\partial N_{H_2O}} \right]_{N_{H_2O}=0.3 mm}$ around the water vapor resonances at 22.23, 183.31 and 325.15 GHz.

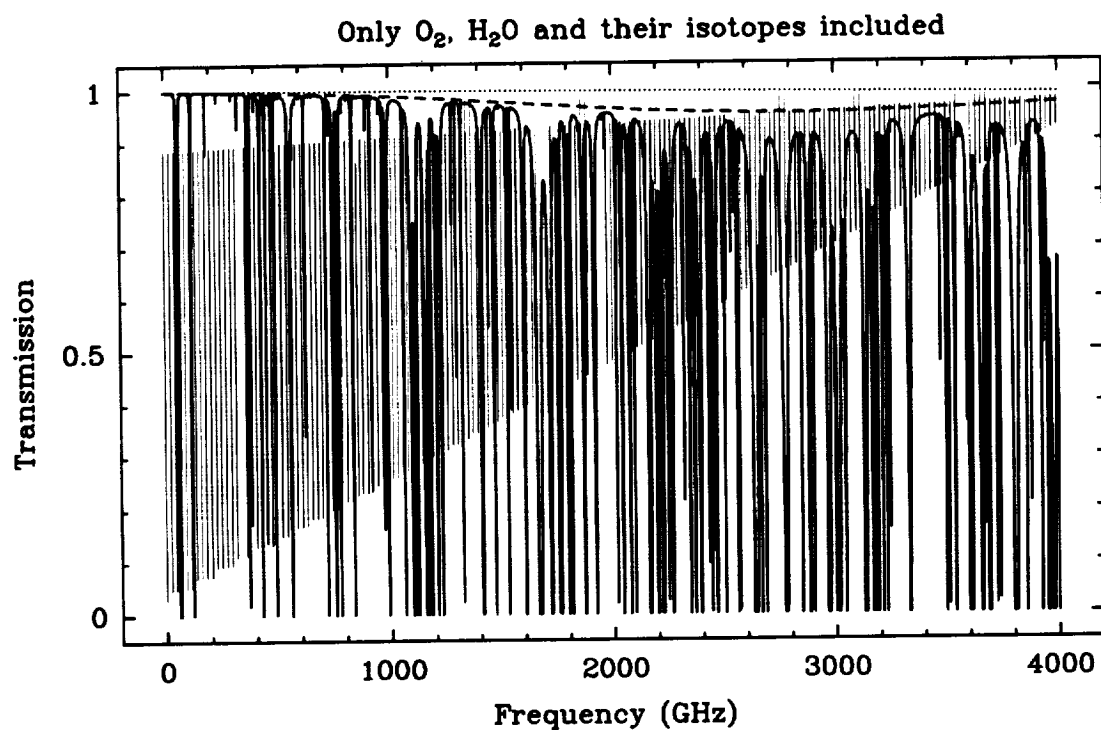


Fig. 6. Atmospheric transmission expected for SOFIA in the range 1-4000 GHz. The trace gases such as O_3 have been removed for clarity (for an idea of their effect, please see next figure). The H_2O pseudocontinuum (dotted line) is expected to be negligible but the dry continuum (dashed line) will contribute up to an opacity of 0.04.

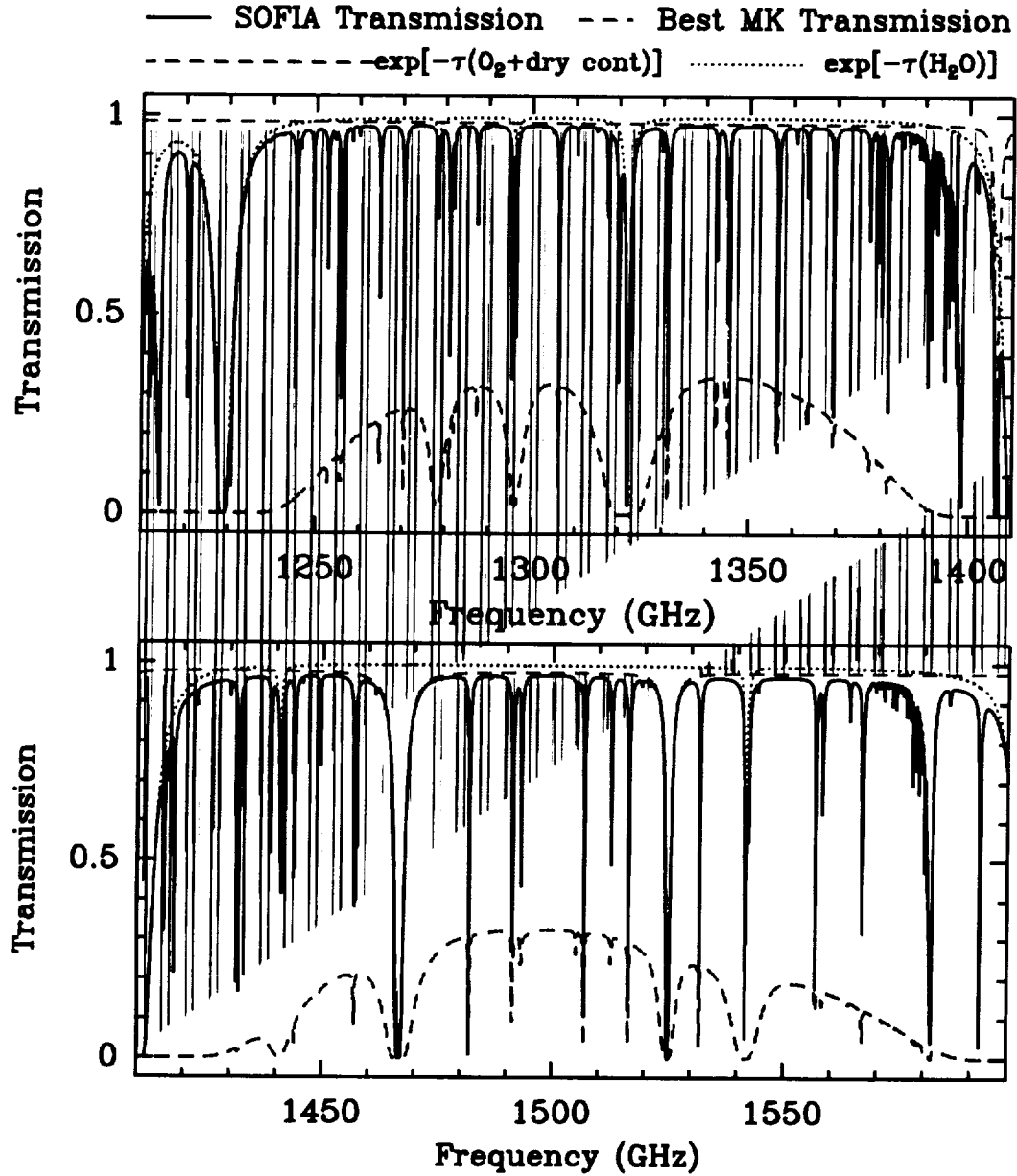


Fig. 7. Zoom of the SOFIA transmission around 1300 GHz and 1500 GHz compared to the transmission expected from the ground in the best ever recorded conditions ($\sim 185 \mu\text{m}$) of water vapor. The local importance of trace gases is stressed in these panels.

